Many-body formulation of the antiferromagnetism of chromium alloys

1990 J. Phys.: Condens. Matter 2 9085

(http://iopscience.iop.org/0953-8984/2/46/009)

J. Phys.: Condens. Matter **2** (1990) 9085–9096. Printed in the UK

Many-body formulation of the antiferromagnetism of chromium alloys

K Schwartzman† and J L Fry‡

† Department of Physics, Indiana University of Pennyslvania, Indiana, PA 15705, USA

‡ Department of Physics, University of Texas at Arlington, Arlington, TX 76019, USA

Received 11 April 1990

Abstract. A tight-binding formulation of the many-body enhanced paramagnetic spin susceptibility derived within the local-density approximation is applied to the antiferromagnetism of Cr alloys. The effects of alloying on the band structures are modelled by a Slater–Koster version of the coherent-potential approximation and matrix elements are computed directly using an averaged linear-combination-of-atomic-orbitals treatment. Antiferromagnetic ordering of the ground state, manifested by a spin-density wave of non-zero wave vector, is predicted when the zero-temperature static susceptibility exhibits a singularity for that wave vector. The spin-density-wave wave vectors computed using this method for dilute $Cr_{1-x}V_x$ and $Cr_{1-x}Mn_x$ alloys are in good agreement with neutron scattering measurements of the wave vectors as functions of impurity concentration. For larger concentrations of impurities, predictions of magnetic order can be made for alternate cubic structures of other 3d transition metals, whose novel structural phases might be stabilized by alloying. In the case of $Cr_{1-x}Mn_x$, a transition to ferromagnetism is predicted for $x = 0.5$. Stabilization of $Cr_{1-x}Mn_{x>0.5}$ in the simple BCC crystal structure could permit an experimental test of an earlier prediction of ferromagnetism in δ-Mn.

1. Introduction

The incommensurate antiferromagnetism of Cr alloys was first observed over twenty years ago in neutron scattering experiments [1]. Pure Cr itself is well known as an antiferromagnet [2] with a spin-density wave (SDW) wave vector, q_{SDW}, of 0.95 $(2\pi/a)$ [100] at low temperatures. An early contribution to the understanding of this phenomenon is due to Overhauser [3] who showed that the electron gas treated within the Hartree–Fock approximation is unstable toward antiferromagnetic order with q_{SDW} equal to $2k_F$. But the Hartree–Fock approximation includes interactions according to the bare Coulomb potential and completely neglects correlations so that its applicability to numerical calculations for real systems is somewhat limited. Nevertheless, later work by Lomer [4] found that the SDW wave vector corresponded almost exactly to the nesting wave vector of two sheets of the Fermi surface (the electron jack centred about Γ and the hole octahedron centred about H) as shown in figure 1. As a result of the nesting, even random-phase-approximation (RPA) formulations [5, 6] of the paramagnetic susceptibility, for example, contain a small energy denominator over a substantial portion of the Brillouin zone. This leads to a peak in the susceptibility at the nesting wave vector, this peak becomes a logarithmic singularity for perfect nesting.

0953-8984/90/469085 + 12 $03.50

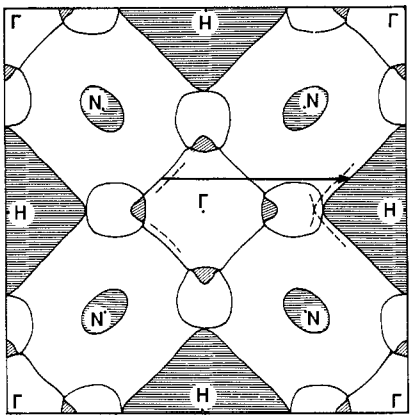

Figure 1. Cross section of the Fermi surface of Cr in the [100] plane. The nesting wave vector for the electron jack about Γ and the hole octahedron about H is indicated; also note the small hole pockets about N and $(0.3,0,0)(2\pi/a)$. With the addition of V impurities, the electron surface contracts and the hole surface expands causing a decrease in the magnitude of the nesting wave vector.

Since the free-energy decrease associated with a transition to the antiferromagnetically ordered phase is proportional to the RPA susceptibility, a global maximum in this quantity (from a peak, for example) at some non-zero wave vector is suggestive of an SDW ground state with that wave vector.

For dilute concentrations of impurities in Cr, it may be reasonably assumed that the band structure and the Fermi surface topology of pure Cr are not substantially altered. The discussion in the previous paragraph can then be extended to explain in simple qualitative terms the incommensurate antiferromagnetism observed in alloys of Cr. For impurities with fewer electrons than Cr, the volume enclosed by electron sheets of the Fermi surface decreases relative to pure Cr while the volume of hole sheets increases. Consequently, the SDW wave vector for $Cr_{1-x}V_x$ alloys can be expected to decrease with increased impurity concentration as indicated in figure 1. Mn impurities, with a greater number of electrons than Cr, result in SDW wave vectors that increase with concentration. Similarly, iso-electronic alloying species such as Mo should have a much weaker effect on q_{SDW} apart from the local volume changes associated with the more massive impurities; this problem is not considered in the present study. RPA calculations of the paramagnetic susceptibility have been performed for dilute alloys of Cr with V and Mn [6], as well as Mo [7], as a function of concentration. The wave vectors of the peaks in the susceptibility follow the discussed trends in very good agreement with neutron scattering [1] SDW wave vectors.

Despite the relative success of the RPA treatment of Cr alloys, the antiferromagnetic ground state can be reliably expected to occur only if the computed paramagnetic susceptibility is unphysical (i.e., it is singular or negative). Moreover, since itinerant magnetism is intrinsically a many-body phenomenon, the formulation of the susceptibility must include electronic exchange and correlation in order to provide a quantitative description of real systems. As discussed more completely in the next section, a magnetic instability with wave vector $\boldsymbol{q}$ is predicted if the many-body enhanced susceptibility exhibits a singularity for that wave vector. Even a simple Stoner model, for example, is sufficient to produce a singularity in the susceptibility (even though it cannot guarantee one). Nesting and matrix element effects must also be considered, although many-body interactions are ultimately responsible for the magnetic instability. A treatment in which exchange and correlation effects are self-consistently included within the local-density approximation has already yielded excellent agreement with

experiment for the SDW wave vector of pure Cr and produced predictions of magnetic order in δ- (simple BCC) and γ- (simple FCC) Mn [8], and has also predicted antiferromagnetism in expanded BCC Ti [9]. The purpose of the present study is to provide an extension of this many-body formulation of the paramagnetic susceptibility to study the antiferromagnetism of alloys, Cr alloys in particular.

Previous theoretical work on the antiferromagnetism of Cr alloys can be resolved into two approaches. The first is based on the choice of a model mean-field Hamiltonian in which imperfect nesting of two bands is assumed [10]. It can produce reasonable agreement with experimental SDW wave vectors, as well as other properties of the antiferromagnetic ground state. The other approach probes, using essentially a first-principles calculation, the paramagnetic susceptibility for magnetic instabilities [6]. While this method employs an RPA formulation, it does not require empirical parameters or assumptions about the details of the band structure.

The second approach is extended in the present work to include many-body interactions self-consistently. Such an approach is not only of interest for studying alloys, but is also of substantial practical value for determining the spin wave spectrum from the dynamic susceptibility and predicting magnetic transition temperatures, subjects of a future studies. The formulation of the many-body enhanced susceptibility and its method of calculation will be discussed in the next section. Results of the calculation are presented and discussed in section 3.

2. Formulation

In order to determine $\boldsymbol{q}_{\mathrm{SDW}}$ for Cr alloys, the many-body enhanced paramagnetic susceptibility is examined for an instability toward antiferromagnetic order. Since the susceptibility is a response function, an instability occurs either at the point the computed susceptibility exhibits a singularity or for a region of the Brillouin zone in which it is negative. Since a singularity will generally not appear without a change in sign of the susceptibility, $\boldsymbol{q}_{\mathrm{SDW}}$ is not uniquely determined since it could be located anywhere in the region of the zone which contains the singularity (or singularities) and a negative susceptibility. However, it may be reasonably assumed that if the wave vector of the singularity corresponds to a peak in the RPA susceptibility, that wave vector is in fact $\boldsymbol{q}_{\mathrm{SDW}}$. In this case the magnetically ordered ground state is characterized by a spatial spin-density oscillation with a wavelength $2\pi/q_{\mathrm{SDW}}$ in the appropriate direction. This approach is an effective, nearly first principles, method for predicting the existence and properties of magnetically ordered systems without the difficulties inherent in a total energy calculation.

In the simplest application of the Stoner model, the enhanced susceptibility is written in terms of the RPA susceptibility χ^0 according to

$$\chi(\boldsymbol{q}) = \chi^0(\boldsymbol{q})/(1 - \Lambda\chi^0(\boldsymbol{q})) \tag{1}$$

where Λ contains exchange and correlation effects arising from particle–hole interactions in the polarization bubble. The quantity Λ has traditionally been assumed to be either constant or to have some relatively simple $\boldsymbol{q}$ dependence. However, a self-consistent formulation of χ has recently been developed [8, 11] in which the three quantities in (1)—χ^0, Λ, and χ—becomes matrices on the reciprocal lattice basis. For

practical purposes, it is more convenient to express χ by transforming (1) into its equivalent form on the orbital basis,

$$\chi(\boldsymbol{q}) = \sum_{i,j,m,n} I_{ij}(\boldsymbol{q})\Gamma_{ij,mn}(\boldsymbol{q})I_{mm}(-\boldsymbol{q}) \tag{2}$$

where the summation indices run through the basis states (in this case 9:1s, 3p, and 5d), I_{ij} is the atomic form factor, and the Γ matrix takes the form

$$\Gamma_{ij,mn}(\boldsymbol{q}) = \sum_{l,l'} \gamma_{ij,ll'}(\boldsymbol{q})[(1 - X(\boldsymbol{q}))^{-1}]_{ll',mn}. \tag{3}$$

The RPA susceptibility matrix γ is given by

$$\gamma_{ij,mn}(\boldsymbol{q}) = -\frac{1}{N}\sum_{\boldsymbol{k},\mu,\nu} \frac{f_{k,\mu} - f_{k+q,\nu}}{E_{k,\mu} - E_{k+q,\nu}} A_{i\mu}(\boldsymbol{k})A_{j\nu}(\boldsymbol{k}+\boldsymbol{q})A_{n\nu}(\boldsymbol{k}+\boldsymbol{q})A_{m\mu}(\boldsymbol{k}) \tag{4}$$

where $E_{k,\mu}$ is the band energy for the electron stage $\boldsymbol{k}$ and band index μ, $A_{k,\mu}$ is the corresponding eigenvector, and $f_{k,\mu}$ is the equilibrium Fermi occupation factor. The wave vector sum runs over the full Brillouin zone, and its method of calculation will be discussed below. The X-matrix appearing in (3) is given by

$$X_{ij,i'j'} = \sum_{\substack{s,t \\ l,m}} I_{ij}(-\boldsymbol{q}_s)\Lambda(\boldsymbol{K}_s - \boldsymbol{K}_t)I_{lm}(\boldsymbol{q}_t)\gamma_{lm,i'j'} \tag{5}$$

where Λ may be decomposed into the product of a solid angle integration and a scalar radial part:

$$\Lambda_{ij,ll'} = \lambda \int K_l^*(\hat{\boldsymbol{r}})K_j(\hat{\boldsymbol{r}})K_l^*(\hat{\boldsymbol{r}})K_{l'}(\hat{\boldsymbol{r}})\,\mathrm{d}\Omega. \tag{6}$$

K_n is a Kubic harmonic (and, in turn, a linear combination of spherical harmonics) and so the angular integral can be evaluated analytically, independent of material parameters or impurity concentration in an alloy. The radial part λ is determined, within the local-density approximation, by the exchange and correlation potential used, in principle, in computing the band structure. It may be written

$$\lambda = \frac{1}{4}\int \mathrm{d}^3r\, r^2 R^4(r) \sum_{\sigma,\sigma'} \sigma\sigma' \frac{\partial V_{\mathrm{xc}\sigma}}{\partial \rho_{\sigma'}} \tag{7}$$

where $V_{\mathrm{xc}\sigma}$ is the exchange and correlation potential for the spin σ, ρ is the local electron charge density, and $R(r)$ is the radial part of the neutral-atom d-state wave function. This integral is an intrinsic property of a metal in a given crystal structure and can be computed independently of the susceptibility calculation. For this purpose, the spin-polarized exchange and correlation potential of von Barth and Hedin [12] is employed, or the potential actually used in computing the band structure, and charge densities are obtained from the tables of Moruzzi, Janak and Williams [13].

The elements of the form factor matrix appearing in (2) may be written [11]

$$I_{ij}(\boldsymbol{q}) = \delta_{ij} I^{(0)}(\boldsymbol{q}) - 5I^{(2)}(\boldsymbol{q}) c_{ij}^{(2)}(\hat{\boldsymbol{q}}) + 9I^{(4)}(\boldsymbol{q}) c_{ij}^{(4)}(\hat{\boldsymbol{q}}) \tag{8}$$

where $\hat{\boldsymbol{q}}$ is a unit vector in the direction of $\boldsymbol{q}$, the c_{ij} are polynomials which may be evaluated directly [11], and

$$I^{(\ell)}(\boldsymbol{q}) = \int_0^\infty r^2 R^2(r) j_\ell(qr)\, \mathrm{d}r \tag{9}$$

in which j_ℓ is a spherical Bessel function. As appropriate for 3d metals, only $\ell = 0, 2, 4$ contribute to the integral and $R(r)$ may be parametrized in the form

$$R(r) = \sum_j \alpha_j r^2 \, \mathrm{e}^{-\zeta_j r} \tag{10}$$

where the quantities α_j and ζ_j are tabulated [14]. However, in the present calculation, the ζ_j are rescaled by solving the radial Schrödinger equation subject to the constraint that 95% of the wave function is in the muffin tin sphere, consistent with the assumption of no overlap of the d-orbitals. The α_j are then determined variationally using the self-consistent band structure potential. Since (10) cannot realistically represent the relatively free s and p electron states (which are treated as plane waves in computing the form factor), it should be observed that only the d states are enhanced by many-body effects in all of the contributions to the susceptibility given in (2). While this has the inherent shortcoming of introducing (most likely relatively small) errors into the numerical results, the qualitative features, primarily the instability towards magnetic order, will not be affected. This is a result of the fact that the itinerant magnetic behaviour of transition metals is due fundamentally to the electronic d-state character of these systems.

Other aspects of this formulation have been discussed elsewhere [8, 11] and the primary reason for its review here is to extend the treatment to dilute alloys. For this purpose, it can reasonably be assumed that three quantities are altered from their values in pure Cr by the presence of impurity species: the band structure, the atomic form factor, and the exchange and correlation integral. The calculation of the band structure in metallic alloy systems, including dilute alloys, from first principles is a considerable undertaking, and is not yet mature enough to be considered reliable. For this reason, as well as computational convenience, Slater–Koster band structures, determined from accurate fits to first principles calculations, are used in the present study. Their use permits scaling properties of the atomic orbital overlap integrals to be exploited in a version of the coherent potential approximation [15]. First, the averaged lattice constant for the alloy $Cr_{1-x}M_x$ where M is an arbitrary metal, is defined to be

$$a = (1 - x)a_{Cr} + xa_M \tag{11}$$

where a_{Cr} and a_M are the lattice constants for pure Cr and M, respectively, and x is the impurity concentration. The scaling scheme of Harrison [16] can now be applied to the overlap integrals of the pure metals. Denoting by ν_{Cr} a given overlap integral for Cr, the corresponding alloy parameter is given by

$$\nu_{Cr_{1-x}M_x} = (1 - x)\left(\frac{a}{a_{Cr}}\right)^n \nu_{Cr} + x\left(\frac{a}{a_M}\right)^n \nu_M \tag{12}$$

where n is -2 for s–s, s–p and p–p bonds, $-7/2$ for s–d and p–d bonds, and -5 for d–d bonds. These new parameters are then used to calculate the band structure of the alloy.

Since the form factor is essentially an atomic quantity, it too is proportional to the respective number densities of host and impurity atoms. The alloy form factor is therefore approximated by

$$I_{ij}^{\mathrm{Cr}_{1-x}\mathrm{M}_x}(\boldsymbol{q}) = (1-x)I_{ij}^{\mathrm{Cr}}(\boldsymbol{q}) + xI_{ij}^{\mathrm{M}}(\boldsymbol{q}). \tag{13}$$

The last quantity to characterize in the alloy is the exchange and correlation integral. This is, in principle, as difficult a problem as the accurate calculation of the alloy band structure. However, since the local-density approximation is successful in accounting for the electronic properties of pure metals, it is reasonable to assume that it is appropriate for use in *dilute* alloys. For this reason, the exchange and correlation integral is treated here as an averaged quantity in the same spirit as the form factor:

$$\lambda^{\mathrm{Cr}_{1-x}\mathrm{M}_x} = (1-x)\lambda^{\mathrm{Cr}} + x\lambda^{\mathrm{M}}. \tag{14}$$

Equations (11)–(14) can be justifiably expected to represent accurately their respective quantities for dilute random alloys of Cr with the impurity species neighbouring Cr on both sides in the periodic table, although (14) is probably the least accurate. It can be argued that the slope of λ would in fact be smaller than that given by (14) for dilute alloys simply *because* of the local-density approximation, a point which will be explored in the following section. With this in mind, the formulation of the dilute alloy problem is complete.

To a somewhat lesser accuracy, the requirement of dilute impurity concentrations can be relaxed for the alloy band structures since in this calculation the lattice constants of V (5.72 atomic units) and Mn (5.2 atomic units) are within 10% of the lattice constant of Cr (5.4456 atomic units). Consequently, the band structures generated using (11) and (12) are probably about as accurate as the fitting procedure would be to a hypothetical first-principles alloy band structure for any x, $0 < x < 1$. In the same spirit, it is therefore also reasonable to expect that I_{ij} and λ may be approximated by (13) and (14), respectively, for any x.

In order to compute the susceptibility, it has already been noted that Slater–Koster band structures are utilized as a convenience. For Cr, an orthogonal two-centre Slater–Koster fit [17] to an LCAO band structure [18] is made for six bands (the one s and five d bands) and 506 $\boldsymbol{k}$ points in the irreducible (1/48) wedge of the Brillouin zone. The fit has an RMS error of 13.7 mRyd overall and is considerably more accurate in the vicinity of the Fermi surface, correctly reproducing the density of states and Fermi energy obtained from the first principles band structure. A similar fit to a scalar relativistic APW band structure [19] for V, using 6 bands and 55 $\boldsymbol{k}$ points in the irreducible wedge, has an RMS error of 4.4 mRyd. For Mn, the (6 band, 506 $\boldsymbol{k}$ point) fit is made to an LCAO band structure [20] computed in the simple BCC phase; although the equilibrium low-temperature crystal structure of Mn is a complex BCC phase with 29 atoms per unit cell, the use of a BCC band structure is justified by the fact that the dilute Cr alloys retain the BCC crystal structure of pure Cr. Secondly, simple BCC Mn is of interest in its own right since it has been predicted to be ferromagnetic [8].

The first, and most time consuming, part of the problem is the calculation of the γ-matrix defined in (4). It has a form very similar to the RPA susceptibility and the method employed to compute it is virtually the same as that discussed in detail in [6]. Only the irreducible wedge of the Brillouin zone must be considered since the transformation properties of the band energies and eigenvectors can be used to accomplish the full zone summation. The sum over the irreducible wedge is carried out using the analytical tetrahedron method [21] in which the wedge volume is decomposed into an integral set

of non-overlapping tetrahedra. Since the calculation is done at zero temperature, the regions of occupied and unoccupied states can be determined by the intersection of the Fermi surface and a given tetrahedron; in the limit of a sufficiently large number of tetrahedra the intersecting surface may be accurately approximated by a plane. In this limit, it is also reasonable to assume that the matrix elements vary slowly enough over a tetrahedron that is only necessary to use their averaged value. Calculations of the susceptibility in which matrix element variation is included in an extension of the analytical tetrahedron method [22] result in corrections of less than a few per cent in all symmetry directions both in the vicinity of a singularity and not. Consequently, advantage can be taken of the considerable savings in computing time obtained by neglecting explicit matrix element variation in a given tetrahedron. The results reported here have been calculated using 506 $\boldsymbol{k}$ points, which correspond to 2000 tetrahedra, in the irreducible wedge of the zone. Comparison of the results for selected wave vectors using finer meshes of $\boldsymbol{k}$ points (up to 1496 $\boldsymbol{k}$ points and 6750 tetrahedra) differ by less than 1% along any of the BCC symmetry directions, including the neighbourhoods of singularities. The remainder of the calculation involves a relatively modest number of matrix manipulations and is straightforward. The entire calculation takes approximately three minutes on a Cray YMP for a wave vector in the [100] direction.

3. Results and discussion

The RPA scalar susceptibility has been studied in some detail in [6] and is important for comparison with the susceptibility enhanced with electronic exchange and correlation effects as discussed above. In terms of the matrix forms given in (4) and (5), the RPA susceptibility may be written

$$\chi^0(\boldsymbol{q}) = \sum_{ij,mn} I_{ij}(\boldsymbol{q})\gamma_{ij,mn}(\boldsymbol{q})I_{mn}(-\boldsymbol{q}) \tag{15a}$$

that is

$$\chi^0(\boldsymbol{q}) = -\frac{1}{N}\sum_{\boldsymbol{k},\mu,\nu} \frac{f_{k,\mu} - f_{k+q,\nu}}{E_{k,\mu} - E_{k+q,\nu}} |M_{\mu\nu}(\boldsymbol{k}, \boldsymbol{k}+\boldsymbol{q})|^2 \tag{15b}$$

where the matrix elements are defined by

$$M_{\mu\nu}(\boldsymbol{k}, \boldsymbol{k}+\boldsymbol{q}) = \sum_{i,j} A_{i\mu}(\boldsymbol{k})I_{ij}(\boldsymbol{q})A_{j\nu}(\boldsymbol{k}+\boldsymbol{q}). \tag{16}$$

A plot of χ^0 and the many-body enhanced susceptibility along the [100] direction for $Cr_{0.99}V_{0.01}$ is shown in figure 2. $\chi^0(\boldsymbol{q})$ exhibits a well-defined peak at about $0.956(2\pi/a)$ which is consistent with the decrease of the nesting wave vector of the electron jack and hole octahedron Fermi surface sheets expected for vanadium alloys. The peak is suggestive of an antiferromagnetic ground state with $\boldsymbol{q}_{SDW} = 0.956(2\pi/a)$ [100]; although this is larger than the observed SDW wave vector of $0.95(2\pi/a)$, it is appropriately smaller than the RPA prediction of $0.9635(2\pi/a)$ for pure Cr (see the discussion in [6] that pertains to this matter). There is also a broad peak centered about $0.65(2\pi/a)$ (not shown) which actually has a larger amplitude than the one at $0.956(2\pi/a)$ and, by the argument in the introduction, should be located at the SDW

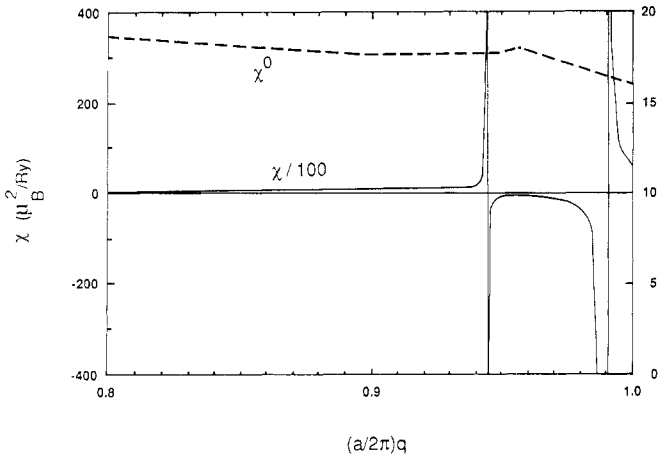

Figure 2. RPA (right-hand scale) and many-body enhanced (left-hand scale) susceptibilities for $Cr_{0.99}V_{0.01}$ as a function of wave vector in the [100] direction. The region of the q axis is chosen to accentuate the important features of these curves; there is also a broad peak in χ^0 centred about 0.65 as discussed in the text. χ^0 in the limit $q = 0$ correctly recovers the electronic density of states at the Fermi surface as found in a separate calculation.

position. However, the magnitude of the broad peak, which arises from the competition between intra- and inter-band scattering, is exaggerated due to the simple plane wave treatment of the s- and p-state contributions to the matrix elements. This, together with the nesting feature, and the fact that a logarithmic singularity may be easily masked numerically, strengthens the prediction of $0.956(2\pi/a)$ as the SDW wave vector. Treating the problem in this manner has a substantial predictive value and has been effectively used in earlier work [5, 6], but the absence of a singularity in the susceptibility weakens the prediction. Secondly, the nesting of Fermi surface sheets is *not* a necessary condition for the appearance of a singularity in the enhanced susceptibility, and a singularity may occur without a corresponding peak in the RPA susceptibility.

The enhanced susceptibility is singular at $0.9448(2\pi/a)$ [100], and exhibits a second pole at $0.99(2\pi/a)$ [100]. Since the susceptibility is negative in the region between the two poles, it could be concluded that the system is unstable against the formation of an SDW ground state for any wave vector in this region. However, the first singularity occurs in the immediate vicinity of the RPA peak, and it may be reasonably deduced that $\boldsymbol{q}_{SDW}$ is the wave vector of that singularity (given the obvious importance of nesting in the antiferromagnetism of Cr and its alloys). This point will be discussed in more detail below.

Similar behaviour is seen in the susceptibilities of other $Cr_{1-x}V_x$ alloys with the predicted SDW wave vector decreasing linearly with increasing x as plotted in figure 3. The wave vector of the second singularity, however, does not follow an easily discernible trend and varies between $0.95(2\pi/a)$ and the zone boundary for the range of x shown in figure 3. In addition, its position is also highly sensitive to the exchange and correlation integral used in the calculation. Changes of a few per cent in λ can cause the two singularities to nearly merge, or push the second one beyond the zone boundary. Despite these variations, the position of the first singularity changes by considerably less than 1%, justifying its choice as the SDW wave vector.

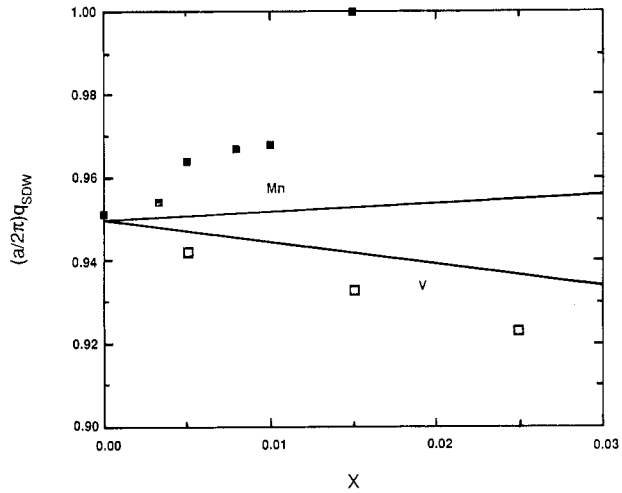

Figure 3. Concentration dependence of q_{SDW} (in the [100] direction). The results of the present calculation (with λ obtained from (14)) are plotted as solid curves, and the neutron data of [1] by open (for V impurities) and closed (for Mn impurities) squares. The q axis origin has been chosen to exaggerate the differences between theory and experiment.

For $Cr_{1-x}Mn_x$ alloys, a double pole structure does not emerge for any x or change in λ. One singularity appears, with a wave vector which increases linearly with x (see figure 3), and the susceptibility is negatively between it and the zone boundary. The position of the singularity is also relatively insensitive to small changes in λ, moving by much less than 1%. In the same spirit as the earlier discussion for V impurities, the SDW wave vector is determined from the location of the singularity.

In the plots of q_{SDW} as a function of concentration shown in figure 3, the solid lines are the result of the present calculation and the open and closed squares are the low temperature neutron scattering SDW wave vectors reported in [1] for $Cr_{1-x}V_x$ and $Cr_{1-x}Mn_x$, respectively. The agreement between the computed and measured wave vectors is very good overall, with exact agreement for pure Cr. However, while the computed slopes of the (approximately) linear dependences on concentration agree closely with the RPA slopes found in [6], there are differences with the observed results. These differences cannot be accounted for, as suggested above, through variation of the exchange and correlation integral, even to the extent of using the pure Cr value of λ. It is therefore likely that the lack of an appropriately computed many-body λ is not the cause of the discrepancies. Similarly, local-field corrections, arising from the rapid spatial oscillation of the spin-density wave, are probably small, particularly in light of the excellent agreement between theory and experiment for pure Cr. This opens the question of the data itself. There is scatter in the spin-density-wave wave vectors obtained in [1] as function of concentration, especially for Mn impurities, and uncertainties in the measured results are not quoted. Together with the vintage of these measurements and the lack of more recent results, a new set of experiments would be beneficial for better understanding these systems and in resolving what may, in fact, be *apparent* discrepancies. It can be concluded that the antiferromagnetism of Cr alloys can be understood in terms of the tight-binding formulation of the paramagnetic susceptibility

presented here, with exchange and correlation enhancements included by means of the local-density approximation.

As an additional point, the results of the present study are computed at zero temperature, but the richness in the temperature dependence of the data presented in [1] has bearing on the present discussion. The observed spin-density wave in pure Cr is transverse between the Néel temperature of 312 K and a 'spin-flip' temperature, T_{sf}, of 120 K. However, below T_{sf} the SDW is observed to be longitudinal. In alloys of Cr, T_{sf} is strongly depressed for increasing impurity concentration, and generally falls below 4.2 K at several atomic per cent concentration. The Néel temperature also decreases rapidly for increasing concentrations of impurity species to the left of Cr (for example, V) in the periodic table, but it increases rapidly for species to its right (for example, Mn). By about a 1% concentration of the latter impurities, an abrupt transition to a commensurate SDW is observed for all temperatures above 4.2 K. It is clear from figure 3 that the computed results would only predict a commensurate spin-density oscillation for considerably larger impurity concentrations (even if λ is allowed to vary as mentioned above). This is not necessarily a failure of the formulation used here, since it is likely that such an abrupt change can only occur if there is an associated structural change in the system.

As might be expected to follow from the discussion in the previous paragraph, the location in the zone of the SDW wave vector also depends on the temperature. The data for $\boldsymbol{q}_{SDW}$ obtained in [1] were generally taken for two sets of temperatures: those close to the Néel temperature and those well below it. In all cases, the wave vectors of the SDW (for incommensurate structures) measured near the Néel temperature were about 1% greater than the corresponding low temperature data, with a smooth variation in between [23]. The temperature dependence of $\boldsymbol{q}_{SDW}$, and the calculation of magnetic transition temperatures, will be treated in a separate publication.

In the present study, the zero-temperature paramagnetic susceptibility is computed and implicitly considers only transverse SDW configurations. However, as noted above, the transverse configuration may not be energetically favourable at $T = 0$ K for any of the alloy compositions under consideration. This distinction could also contribute to the disagreement between the computed and observed wave vectors discussed above; the free energy difference between the transverse and longitudinal SDW configurations can be expected to increase with increasing impurity concentrations (despite the precipitous decrease in T_{sf} which accompanies increasing x).

The susceptibility at the zone centre yields the electronic density of states at the Fermi surface (and comparison with the RPA susceptibility furnishes a computed measure of many-body effects on the density of states or, equivalently, the specific heat). A plot of $\chi(0)$ as a function of concentration of Mn impurities in Cr is shown in figure 4. The rapid increase and subsequent singularity at above equi-atomic concentrations indicates an instability of either the paramagnetic or antiferromagnetic phase (depending on whether there is a pole in the susceptibility at a non-zero wave vector). Since $\chi(0)$ is negative beyond approximately $x = 0.5$, the system is unstable toward formation of a ferromagnetic ground state (which can be thought of a spin-density oscillation with infinite wavelength). This is consistent with an earlier prediction [8] of ferromagnetism in pure δ-Mn and might provide an experimental approach to test that prediction which is simpler than the difficult problem of epitaxial growth of simple BCC Mn [24]. In addition, the susceptibility was also studied for an antiferromagnetic instability for $x < 0.5$: with the alloy λ given by (14) antiferromagnetism was found for $x < 0.27$ which persisted to $x = 0.45$ by allowing variations of several per cent from (14). This

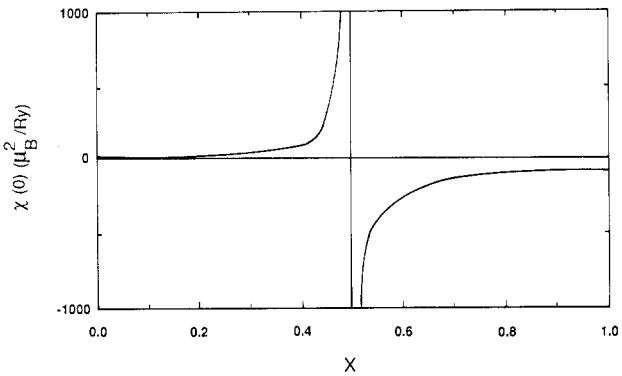

Figure 4. The many-body enhanced susceptibility at the zone centre as a function of x for $Cr_{1-x}Mn_x$. The calculation was actually done for $\boldsymbol{q} = 0.00005,0,0)(2\pi/a)$ to avoid numerical problems, and (14) was used to determine λ. The singularity at $x \approx 0.5$ indicates a ferromagnetic instability.

is reasonably consistent with the data of [1] which indicates a non-vanishing Néel temperature to $x = 0.5$, although the crystal structure at these concentrations is not specified.

4. Conclusions

The antiferromagnetism of dilute Cr alloys with V and Mn impurities may be treated accurately by means of a tight-binding formulation of the paramagnetic susceptibility with electronic exchange and correlation included self-consistently within the local-density approximation. Agreement between computed and measured results for the SDW wave vector as a function of impurity concentration is very good. The relatively minor discrepancies that occur in the slopes of the (approximate) linear dependences can possibly be attributed to the distinction between the transverse and longitudinal susceptibilities as a function of temperature. However, it can also be argued that a new set of more accurate low temperature measurements of the concentration dependence of $\boldsymbol{q}_{SDW}$ is called for. The success of the approach studied here is consistent with the conventional understanding of the importance of Fermi surface nesting in Cr alloy system, as well as the results of a previous RPA formulation of the problem.

The possibility of alloy stabilization of $Cr_{1-x}Mn_x$ in the simple BCC phase, for approximately equi-atomic concentrations of Cr and Mn, is suggested as a method for experimentally determining whether δ-Mn is ferromagnetic. The present study predicts ferromagnetism in simple BCC $Cr_{1-x}Mn_x$ for $0.5 \leqslant x \leqslant 1$.

Acknowledgments

Computational support provided through a grant from the Pittsburgh Supercomputing Center to one of us (KS) is gratefully appreciated. Support for JF was provided through a grant from the Robert A Welch Foundation.

References

[1] Koehler W C, Moon R M, Trego A L and Mackintosh A R 1966 *Phys. Rev.* **151** 405
[2] Shull C G and Wilkinson M K 1953 *Rev. Mod. Phys.* **25** 100
[3] Overhauser A W 1962 *Phys. Rev.* **128** 1437
[4] Lomer W M 1962 *Proc. Phys. Soc.* **80** 489; 1964 **84** 327
[5] Gupta R P and Sinha S K 1971 *Phys. Rev.* B **3** 2401
[6] Schwartzman K, Fry J L and Zhao Y Z 1989 *Phys. Rev.* B **440** 454
[7] Since Mo is isoelectronic with Cr, the alloy dependence of q_{SDW} is much weaker.
[8] Zhao Y Z, Fry J L, Pattnaik P C and Schwartzman K 1990 *Phys. Rev.* B at press
Fry J L, Zhao Y Z, Pattnaik P C, Moruzzi V L and Papaconstantopoulos D A 1988 *J. Appl. Phys.* **63** 4060
[9] Hartford E, Schwartzman K and Fry J L 1989 *Bull. Am. Phys. Soc.* **34** 649
[10] Machida K 1984 *Phys. Rev.* B **30** 418
Machida K and Fujita M 1984 *Phys. Rev.* B **30** 5284
[11] Callaway J, Chatterjee A K, Singhal S P and Ziegler A 1983 *Phys. Rev.* B **28** 3818
[12] von Barth U and Hedin L 1972 *J. Phys. C: Solid State Phys.* **5** 1629
[13] Moruzzi V L, Janak J F and Williams A R 1978 *Calculated Electronic Properties of Metals* (Oxford: Pergamon)
[14] Clementi E and Roetti C 1974 *At. Data Nucl. Data Tables* **14** 277
[15] Fletcher G, Fry J L, Pattnaik P C and Papaconstantopoulos D A 1988 *Phys. Rev.* B **37** 4944
[16] Harrison W A 1980 *Electronic Structure and the Properties of Solids* (San Francisco: Freeman)
[17] Pattnaik P C, Dickinson P H and Fry J L 1983 *Phys. Rev.* B **28** 5281
[18] Laurent D G, Callaway J, Fry J L and Brener N E 1981 *Phys. Rev.* B **23** 4977
[19] Papaconstantopoulos D A 1980 *Handbook of the Band Structures of Elemental Solids* (New York: Freeman)
[20] Fuster G, Brener N E, Callaway J, Fry J L, Zhao Y Z and Papaconstantopoulos D A 1988 *Phys. Rev.* B **38** 423
[21] Rath J and Freeman A J 1975 *Phys. Rev.* B **11** 2109
[22] Pattnaik P C, Fry J L, Brener N E and Fletcher G 1981 *Int. J. Quantum Chem. Symp.* **15** 499
[23] Werner S A, Arrott A and Kendrick H 1967 *Phys. Rev.* **155** 528
[24] Tian D, Wu S C, Jona F and Marcus P M 1989 *Solid State Commun.* **70** 199
Heinrich B, Liu C and Arrott A S 1985 *J. Vac. Sci. Technol.* A **3** 766
Heinrich B, Arrott A S, Liu C and Purcell S T 1987 *J. Vac. Sci. Technol.* A **5** 1935